Formation of Plastic Strains During Welding of Aluminum Alloys

Moiré fringe dynamic strain analysis shows how large plastic strains form during GTA welding of an Al-Mg alloy

BY LYTLE JOHNSON

ABSTRACT. The principal and shear strains around gas tungsten-arc welds in Al-Mg sheet are measured using a projected-grating moiré fringe strain analysis technique (described in detail In a previous paper). Dynamic strain patterns are recorded during welding using a movie camera. The strain values are plotted as three-dimensional graphs to show clearly how strains develop around the weld pool.

Nine different combinations of welding variables have been repeated three times for increased precision. The temperature distributions for these welding conditions are measured using thermocouples. The results indicate that the straining around the arc consists mostly of shear strain. The normal strains are much smaller. The planes of maximum shear strain are oriented almost exactly parallel and perpendicular to the weld bead. The strain patterns correlate well with the temperature distributions, and a theory is proposed which describes the formation of plastic strains during welding and the influence of welding conditions on strain patterns.

Introduction

During a study of solidification cracking In aluminum alloys it became apparent that most previous research has been aimed at elucidating the metallurgical processes involved. Although the findings from such research have often been quite useful, the fact remains that the metallurgical processes occur while the surrounding plate is undergoing rapid heating and cooling and a phase change (solidification) is taking place. These factors result in a stress-strain pattern which directly affects cracking in and near the weld. This pattern could be expected to vary according to the set of welding parameters used and the mechanical properties of the alloy. Research which does not take into account this mechanical situation is therefore bound to be of limited usefulness.

The need to better understand welding stress and strain patterns is certainly not restricted to solidification cracking problems, nor is this paper the first to concern itself with such patterns. In the past both theoretical and experimental research has been done to determine the magnitude and distribution of welding stresses and strains. The theoretical work has often been unsatisfactory because of the complexity of the situation. Several factors contributing to this complexity are: (1) the physical and mechanical properties of most materials at high temperatures, especially in the region of the solidus, are not well known, (2) these properties are often highly temperature dependent, and (3) heat flow theory is least accurate for the region quite near the weld, which is where the stresses and strains are most important. The experimental research has either simulated the welding process with plastic models or has used strain measuring devices at a small number of points. Between them, these theoretical and experimental investigations have not produced a detailed coherent picture of the formation of welding stresses and strains.

The work described here is an attempt to supply this overall picture. Recent contributions to the field of experimental stress analysis have been applied to the gas tungsten-arc welding of aluminum alloy sheet. The results provide some new thoughts on straining during welding.

Literature

The stress-strain pattern which is formed during welding results from the non-uniform distribution of heat within the metal, with the net effect being localized deformation near the weld. This deformation can cause distortion of entire structures.[1] In general, when the temperature distribution has been determined, the order of magnitude of thermal stress may then be represented by the stress required to suppress free thermal expansion or contraction.[2] Tall[3] describes the formation of welding stresses and strains: as temperatures in the plate increase around the approaching arc, the hottest metal undergoes plastic compression because the cooler surrounding plate prevents its free thermal expansion. Behind the arc both solidification shrinkage and cooling contraction lead to the development of tensile stresses as temperatures and temperature gradients decrease.

An understanding of welding heat flow is therefore necessary when discussing welding stresses and strains Christensen et al[4] summarized the results from a number of previous

LYTLE JOHNSON, formerly in the Metallurgy Dept., University of Strathclyde, Glasgow, Scotland, is presently with Union Carbide Corp., Nuclear Division, Oak Ridge, Tenn. *Paper was presented at the 54th AWS Annual Meeting held in Chicago during April 2-6, 1973.*

papers on the subject and rewrote the heat flow equations in dimensionless form. A comparison of the predictions from these equations with experimental data showed that the discrepancies are most pronounced for points near the weld centerline. This same conclusion was drawn by Meyers et al[5] in one of the most recent published surveys of welding heat flow. In examining distortion of aluminum alloys during welding Kazimirov and Nedoseka[6] found that heat flow theory for points near the weld pool was too inaccurate to be of any use, so they used thermocouples to obtain temperature distributions near the weld.

Boulton and Lance Martin[7] presented one of the first theoretical analyses of welding stresses and were the first to demonstrate that welding causes permanent plastic deformation in the heat-affected zone. However, the analysis did not consider the nature of the stress pattern around the moving arc, and only longitudinal residual stresses were calculated. Tall[3] calculated welding stresses by summing incremental stresses and strains due to the changing temperature distribution as welding progresses, with time being divided into a number of intervals for the calculation. Although this approach comes closer to the actual stiuation than Boulton and Lance Martin's, Tall also calculated only longitudinal stresses and assumed that plane transverse sections through the plate remain plane during welding. Prokhorov[8] and Makhnenko[9] used a computer to simplify calculations similar to Tall's, but they still consider only plane transverse sections. Masubuchi and Ich[10] used a finite-element computer program to calculate stresses near the completed weld. Although the analysis considered transverse welding stresses, the dynamic stress-strain pattern was not included in their approach.

The previous experimental work to determine welding stresses and strains has been divided into post-welding and during-welding groups. Although post-welding measurements are of little use for studying the dynamic stress-strain patterns during welding, a few have been included because they can be used for dynamic measurements.

The post-welding techniques include all residual stress measuring methods, most of which have been adequately reviewed by Dawes.[12] Boulton and Lance Martin[7] and Makhnenko et al[13] measured the change in distances between sets of markings on the plate due to welding. Prokhorov et al[14] examined band patterns around electron beam welds on polished steel surfaces. Dantu[15] and Cargill[16] used moiré fringe techniques and found large (2-4%) residual transverse strains near the weld.

Some of these techniques can also be used during welding. Dyatlov and Sidoruk[17] measured transverse strains near the weld with various types of extensometers. Dechaene et al[18] developed a moiré fringe technique for measuring strain cycles at the tip of a notch cut in the heat-affected zone. Their moiré method was also used by Soete et al[19] in a study of exhaustion of ductility caused by these strain cycles. Some further experimental work has used photoelasticity,[20,21] although it is questionable whether the welding of metals can be simulated in plastics.

Summary

1. For areas near the heat source, direct measurement of welding thermal cycles is probably more satisfactory than calculating thermal cycles from heat flow theory.

2. Existing mathematical methods for calculating welding stresses and strains do not apply to the transient patterns surrounding a moving heat source. The assumptions which are necessary for these calculations are usually not valid in the transient situation.

3. Only a few strain measuring methods can be used for dynamic measurements. Of these, only two, photoelasticity and moiré, are capable of measuring stresses and strains over a large surface area. Photoelasticity is limited by the problem of simulation. Therefore moiré techniques seem to be the most promising for measuring welding strain patterns.

Scope of This Work

The purpose of this research is to measure and characterize the transient strain fields around a moving welding arc. The research program therefore includes the following features:

1. Gas tungsten-arc welding is used without filler metal to minimize variations caused by the welding process.

2. The specimens are made of 3 mm sheet to keep the heat flow and strain patterns essentially two-dimensional.

3. All welds are bead-on-plate to eliminate fit-up as a source of complication.

4. Aluminum alloys have been chosen for the study because they undergo fairly large deformations during welding. In addition, there are no phase changes below the solidus temperature, and the metallurgical structures are not particularly cooling rate sensitive.

An important part of the work is to develop suitable experimental strain analysis techniques for making the necessary measurements. A moiré fringe method is used because it is well suited to high temperature strain analysis and gives all necessary strain data from a single photograph. Temperature distributions around the arc are measured as an aid to understanding the significance of the strain patterns.

Experimentation

All welding coupons were cut from ⅛ in. (3 mm) N6 sheet in the as-received ¼-hard condition. This alloy, with 4.5-5.5% Mg, is quite similar to 5056 or 5356. The rectangular coupons measured 300 × 800 mm, and welds were made along the centerline in the long direction. The top surfaces of the coupons were ground with 600-grade paper along the centerline to ensure uniform surface emission characteristics for the welding arc.

The coupons are prepared for strain measurement by etching a high-frequency grating (500 line/in., or 20 line/mm) onto the bottom of each one, because subsequent superposition of a similar grating on this one will produce an interference pattern of light and dark bands called moiré fringes. The method developed for this work superimposes the two gratings by projecting a remote grating (on glass) onto the bottom of a coupon with etched grating. The grating projection system is built into the welding work table and is shown in Fig. 1.

This system produces a moiré fringe pattern on the bottom of the coupon which can be easily photographed during welding. The fringe pattern will be altered quite drastically as welding takes place because the specimen grating (on the coupon) deforms slightly. A 3 mm reference grid, also etched onto the coupons, greatly simplifies analysis of the moiré patterns. The principles of moiré strain analysis are somewhat involved and are not essential for the present paper, so they are not described here. A complete account can be found in Johnson,[22,23] and Theocaris[24] gives a good account of moiré methods in general.

Gas tungsten-arc (ac) welding with a surge injector and zirconiated tungsten electrodes was used throughout this work. All welds were bead-on-plate with no filler metal. Three currents were chosen for each of three travel speeds — 200, 500, and 800 mm/min, or 8, 20, and 32 ipm — to give weld beads ranging from 50% to full penetration. The nine sets of welding conditions are given in Table 1.

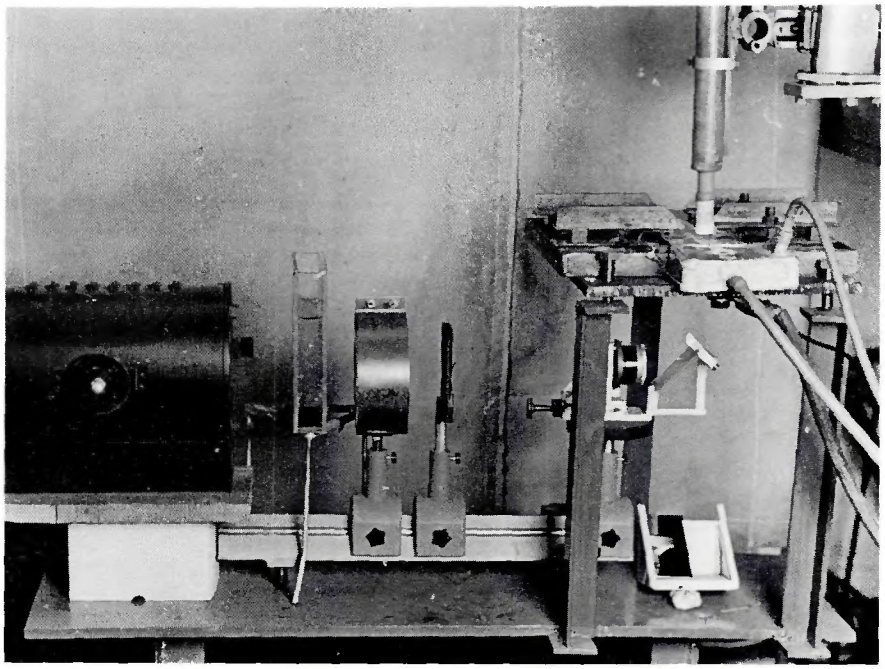

Fig. 1 — The grating projection system and welding work table with cover for light source removed. A specimen is shown mounted in the fixturing device

Each welding condition was repeated three times, and all welds were made in random order to minimize possible effects of uncontrollable time-dependent variables. A 16 mm movie camera filmed first the initial fringe patterns and then the fringe patterns as they changed during welding. Reversal black-and-white film was used because of its high speed (160 A.S.A.). The framing rate was 16 frames/second.

One set of nine welds was made on coupons with thermocouples attached to their undersides. The thermocouple junctions were spot welded in a row across the plate 150 mm from one end and at distances of 7, 12, 17, and 22 mm from the weld centerline. Each thermocouple had its own pair of cold junctions in ice water. (Some preliminary work had shown that a common cold junction for one lead from each couple would not give independent readings for each thermocouple because the hot junctions could not be electrically insulated from each other.) A six-channel ultraviolet light recorder was used to trace the thermocouple outputs.

Results

Individual frames were printed from the films taken of the moiré fringe patterns during welding. Since a quasi-stationary (steady with respect to the moving electrode) temperature distribution occurs during welding of these specimens (see Ref. 5), and since the coupons are of constant width and sufficiently long so that end effects can be ignored, a quasi-stationary strain pattern around the electrode has been assumed. This means that individual prints from the movie film, representing the strain pattern at various times for a fixed area of the specimen, could be thought of as representing various positions on the specimen at a particular time.

This quasi-stationary condition is necessary for this work because the area of good contrast and reasonable sharpness of the fringe pattern was only slightly over 12 mm wide (in the direction of welding) and 18 mm long (transverse to the weld). Therefore three and one-half of these basic analyses were used to give an overall analysis area of 18 mm x 42 mm, as shown in Fig. 2. The initial (prior to welding) fringe pattern was also used in the analysis, and is shown at the left in Fig. 2.

The strain analysis procedure combines these basic analyses mathematically, and normal strains ($\mathcal{E}_x$ and $\mathcal{E}_y$) and shear strains (γ_{xy}) are computed from them assuming small strains and small rotations.[25] Then, using Mohr's two-dimensional strain circle for these small strains, the maximum shear strain, principal strains, rigid-body rotation, and normal strains on the planes of maximum shear strain — γ_{max}, $\mathcal{E}_1$- $\mathcal{E}_2$, α ($\mathcal{E}_x$ + $\mathcal{E}_y$)/2 can be calculated. The three complete sets of strain values from the repeated welds for each set of welding conditions are then averaged. The averaged strain values are presented as three-dimensional graphs over the 18 × 42 mm area adjacent to the weld by using the computer's graph plotter. Figure 4 shows typical strain patterns, and Fig. 3 shows how the graphs are related to the weld bead and torch. The equations and computational details can be found in Ref. 23. Only a few of the results, from two of the welding conditions (105 amp — 200 mm/min and 250 amp — 800 mm/min), have been presented here. The complete results can be found in Ref. 22.

Table 1 — Nine Sets of Welding Conditions Used in Preparing Specimens

Travel speed mm/min	Welding current, amp		
200	105	115	125
500	165	182	200
800	210	230	250

Temperature recorder traces for these two welding conditions are shown in Fig. 5. A distance scale has been added along the bottom of each set. Although the electrode location (the zero point on the distance scale) was not recorded, it could be estimated fairly accurately from the peak of the traces for the thermocouple nearest the centerline. These traces were used to obtain the temperature gradients $\delta T/\delta Y$ (estimated from hand-drawn tangents to the traces, and given in Table 2) and $\delta T/\delta X$ (shown in Fig. 6). Cross-sectional macrophotographs of the three repeat welds made at these same two sets of welding conditions are shown in Fig. 7.

Discussion

Errors

The error in the strain graphs for three averaged welds is approximately 0.003. Most of this error arises from unsharpness in the fringe patterns and the difficulties in assigning numerical values to points of the 3 mm reference grid. Errors from using small strain equations and assuming no out-of-plane deformation of the coupons are probably less than 0.003 and thus detract very little from the accuracy. The largest errors are caused by extrapolation and occur at corners or along the edges of the 18 × 42 mm rectangle.

The temperature recording apparatus was checked by recording cooling curves for several aluminum alloy melts. The agreement with published data for these alloys was quite good, so most of the estimated error of ±5C in Fig. 5 seems to arise from widening of the trace lines during welding. This widening comes from mechanical vibration of the recorder and fluctuating electrical currents in the coupons.[22]

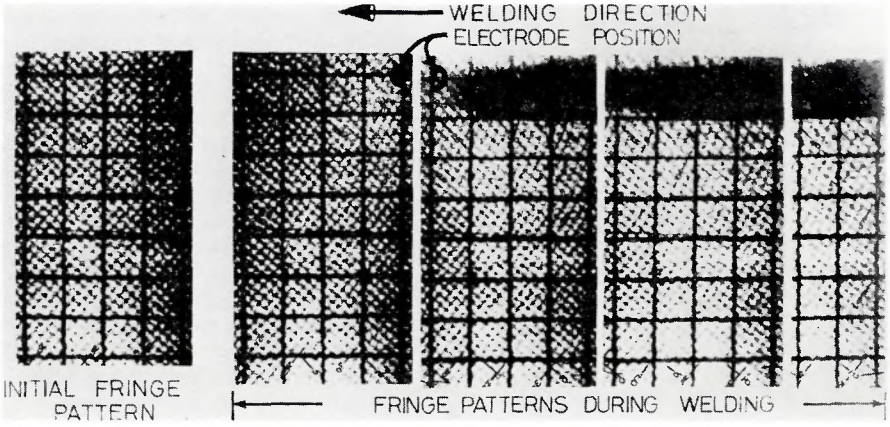

Fig. 2 — Fringe photographs which comprise the experimental results for one weld analysis. The bending of the fringes can be seen by sighting across the page at a shallow angle

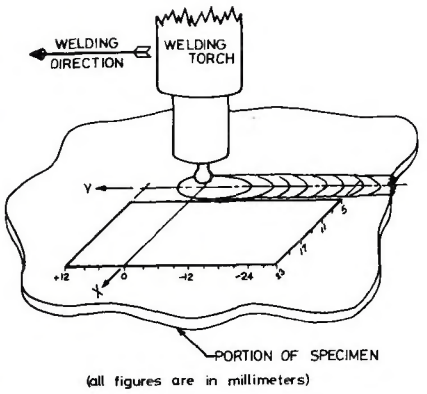

Fig. 3 — The location of the 18 × 42 mm analysis area in relation to the weld bead, weld pool, and moving torch. This diagram shows how the graphs in Fig. 4 are related to the welding process

Temperature Distributions

As welding speed and current increase, there is a marked increase in the temperature gradient ahead of the electrode. Also, as current increases at constant welding speed, the peak temperature experienced at a point near the weld increases. Finally, as travel speed increases (while maintaining as nearly as possible constant penetration), there is a greater temperature gradient at right angles to the direction of welding. This means that at high welding speeds the maximum temperature reached at a point near the weld will be lower than at slower welding speeds. Together with Table 2, Fig. 6 shows that temperature gradients ahead of and on either side of the weld pool are almost doubled when the welding speed increases from 200 mm/min to 800 mm/min.

Welding Strain Patterns

The strain graphs, of which four are shown in Fig. 4, can be more readily understood by first looking at Fig. 3. This figure shows the relation of the 18 × 42 mm analysis area to the weld bead and moving torch, as well as showing how the X and Y axes are oriented and calibrated for this work. The vertical displacements in the graphs are the strain values at points (x, y) in the 18 × 42 mm area. The three-dimensional graphs therefore represent a strain 'surface' over this rectangular area next to the torch. Although only four of the 45 strain graphs have been shown here, the following discussion describes the trends observed in the entire series of welding results.

The normal strain in the X-direction (transverse strain, $\mathcal{E}_x$) has been plotted with negative, or compressive strain upward in order to better show the straining behavior near the weld. The most striking feature of the $\mathcal{E}_x$ plots is the increasingly sharp negative curvature in the strain pat-

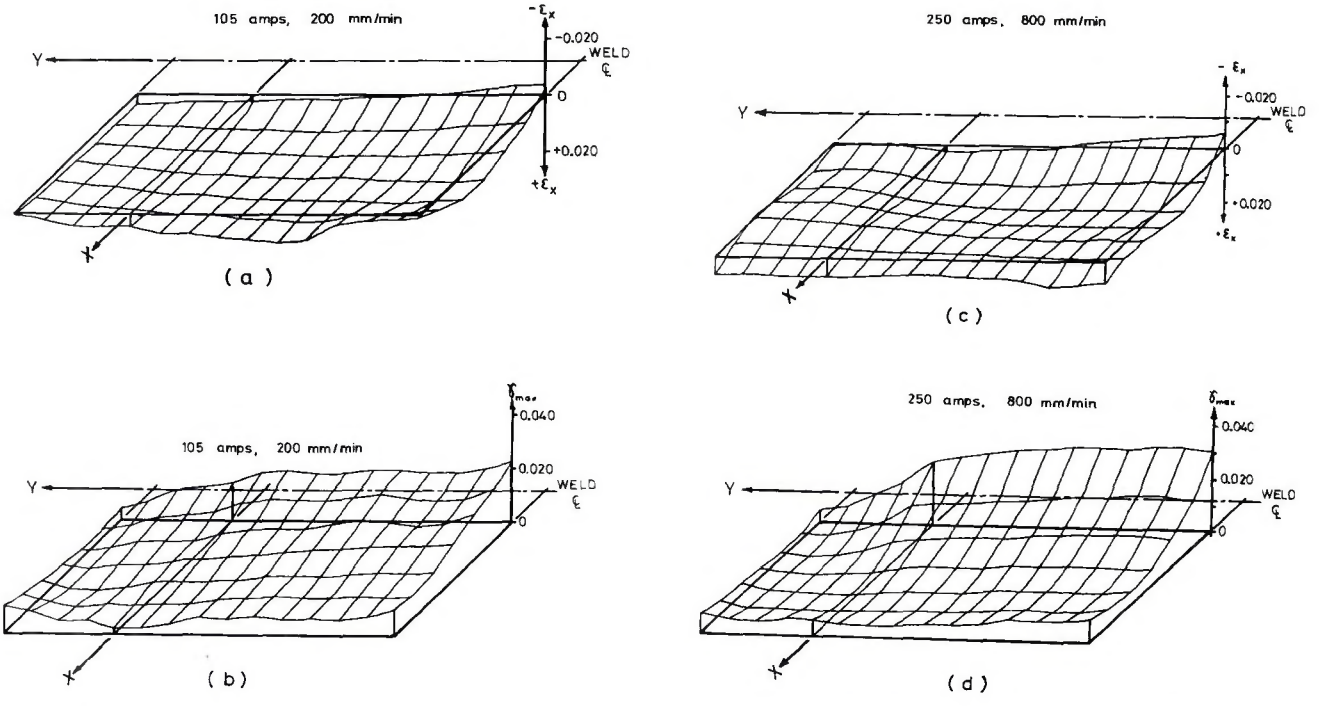

Fig. 4 — Three-dimensional plots of the calculated strains near the weld. (a) and (b) are transverse strain ($\mathcal{E}_x$) and maximum shear strain (γ_{max}) for a low-speed weld, while (c) and (d) are the same graphs for a high-speed weld

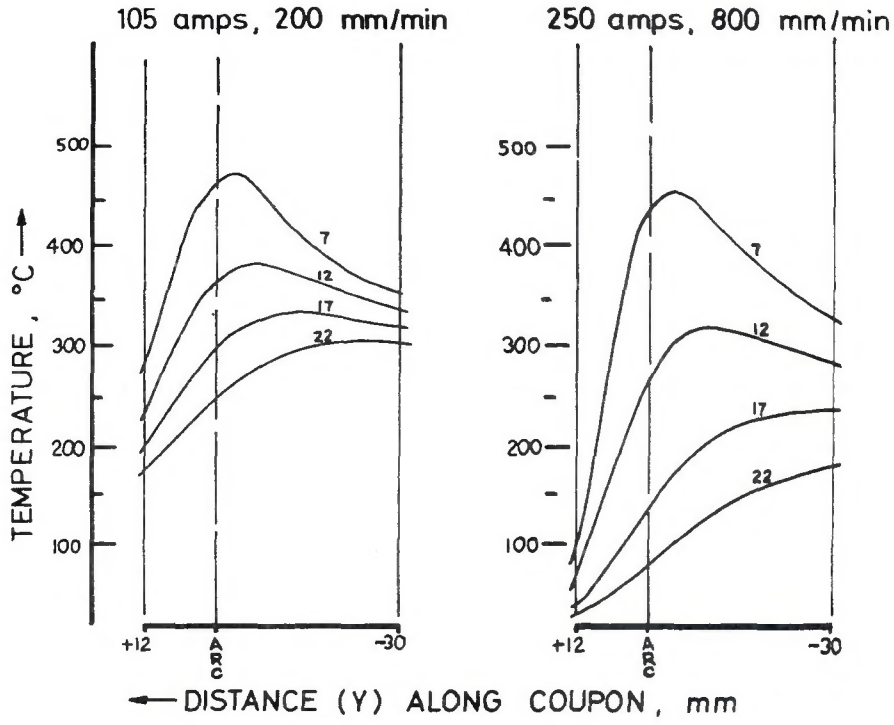

Fig. 5 — Thermocouple temperature traces for two welding conditions. The small figures near each trace give the distance of the thermocouple from the weld centerline (in millimeters)

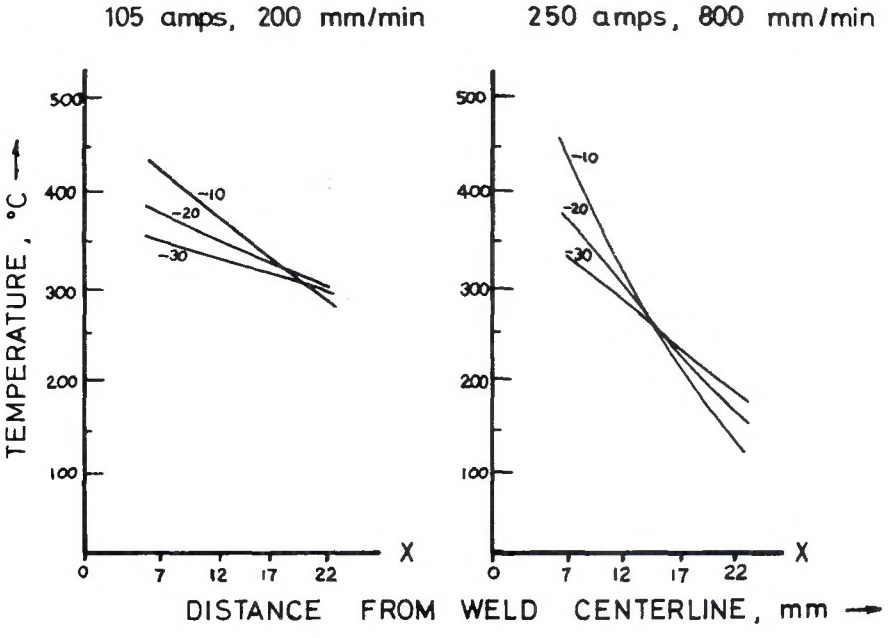

Fig. 6 — Temperature profiles perpendicular to the welding direction at three locations behind the electrode (Y = −10, -20, −30 mm). The data were taken from Fig. 5

Table 2 — Temperature Gradients in Vicinity of the Arc (See Fig. 6)

Travel speed, mm/min	Current, amp	In front of arc	Temperature gradient, $\delta T/\delta y$, C/mm −10mm	−20mm	−30mm
200	105	+20	−6	−4	−2
800	250	+34	−7	−5	−4

terns as welding speed increases. If the coupons were free to expand, in accordance with the temperature distributions, then strains would become more and more positive near the centerline due to thermal expansion. It can be seen from the strain patterns for points away from the weld centerline that this thermal expansion begins to take place, but nearer the centerline a substantial amount of compressive plastic strain occurs. Since near the weld centerline the free expansion would be at least 1½% (0.015), a measured welding strain value of zero would represent 1½% compressive strain at room temperature. The negative welding strain values then represent even more plastic straining. This agrees with the results from Dantu[15] and Dyatlov and Sidoruk.[17] The effect becomes greater at high welding speeds.

The normal strain in the Y-direction (longitudinal strain, ε_y) is generally quite uniform and slightly positive, as would be expected from thermal expansion considerations. The rather small change in ε_y seems to be related to the elongated isotherms associated with welding; the metal near the weld pool could shift rearward, thus avoiding large strain concentrations (this point is discussed in greater detail later). ε_x, on the other hand, could build up near the centerline because of the restraining effect of the cooler metal away from the weld and the steep thermal gradients in the X-direction. The small strain values near the weld are less than would be predicted by free thermal expansion, so compressive plastic straining is predicted by theoretical analyses of welding straining (see Literature section of this paper) and has often been deduced from residual stress studies (for example Ref. 3).

The substantial maximum shear strains (γ_{max}) which are apparent in these results (Fig. 4) have not been mentioned by previous authors except for Cargill.[16] Although Chihoski's[19] discussion of welding strains implies that shear straining should occur, he does not specifically point this out. Maximum shear strain generally increases throughout the analyses as current and welding speed increase. As was the case for ε_x, the shear strain is increasingly confined to the immediate vicinity of the weld as welding speed increases. Thus the gradient of shear strain in the X-direction behaves much like the temperature gradient near the weld pool. The results show that this shear strain shifts points near the weld rearward.

The planes of maximum shear strain are oriented in almost the same directions as the X and Y axes, as shown in Fig. 8. This orientation is about the same for all welding condi-

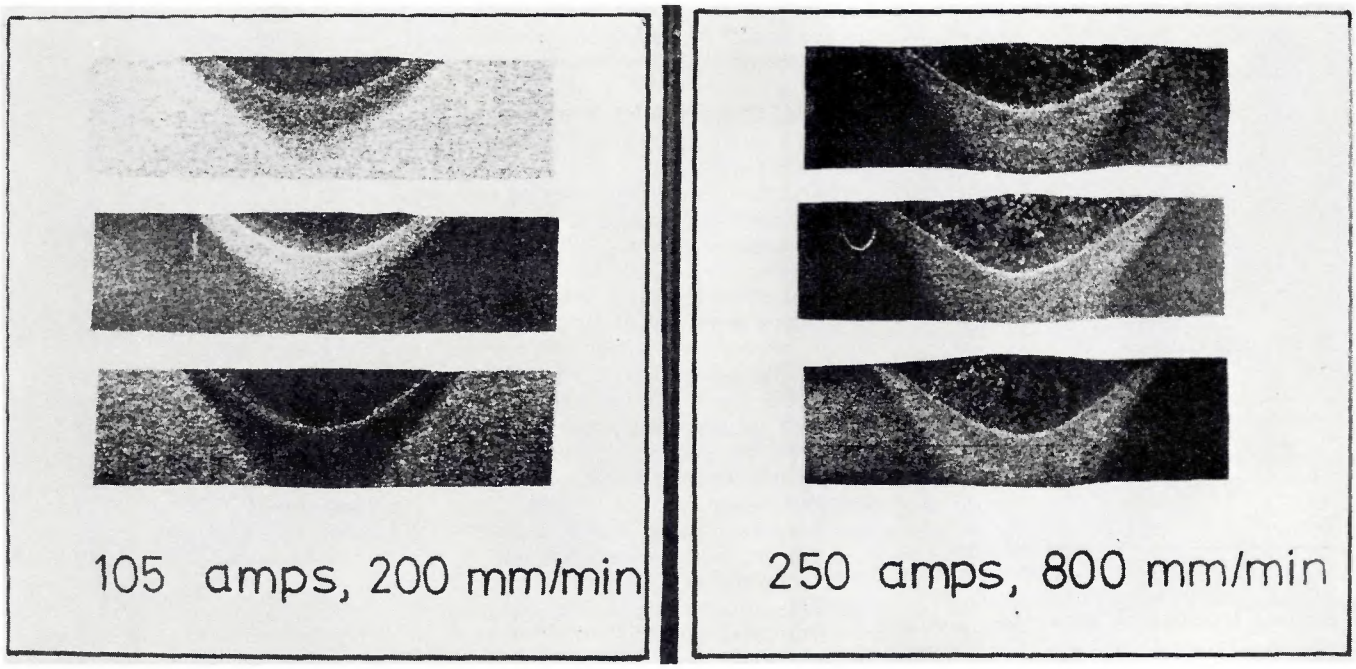

Fig. 7 — Transverse sections of the three repeat welds for two welding conditions (3 mm sheet)

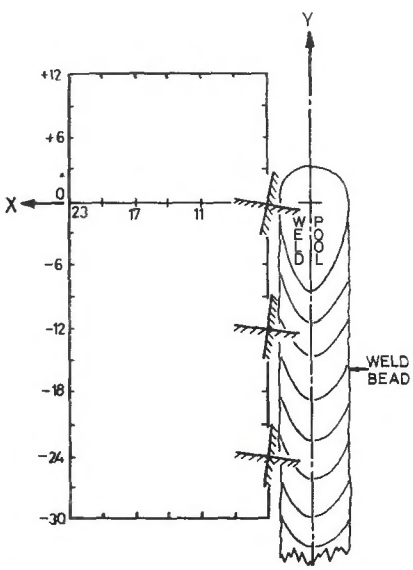

Fig. 8 — The orientation of the maximum shear strain planes for three locations near the weld. Although the results shown are for the 182 amp, 500 mm/min weld, very similar results were obtained for all the welding conditions used

tions and is typical of a situation where γ_{xy} is much larger than the quantity $(\mathcal{E}_x - \mathcal{E}_y)$.

Rigid-body rotation is a measure of the net angular displacement resulting from shear and normal strains. In every case the rotation was such that points near the weld are displaced rearward. (In other words, transverse lines which were straight prior to welding are permanently bent rearward during welding). The rigid-body rotation patterns are quite similar to the γ_{max} strain patterns because the analysis equations interpret this rearward shifting as both shear strain and rigid-body rotation, even though lines originally parallel to the Y-axis have changed very little.

The graphs for the normal strain on the maximum shear planes — $(\mathcal{E}_x + \mathcal{E}_y)/2$ — show a small thermal expansion effect and, as was the case for $\mathcal{E}_x$ and $\mathcal{E}_y$, there has been compressive plastic yielding during welding. As the weld area cools down, the strain becomes negative. Normal strain on the maximum shear strain planes is important because if a large amount of shearing has caused voids to form along grain boundaries oriented on planes of maximum shear strain, the normal stress on these voids or lines of voids can easily cause cracking. (A normal stress could develop, for example, if normal cooling contraction were restrained).

Formation of Plastic Strains During Welding

From the preceding discussion of welding temperature distributions and the various strain patterns around the moving weld pool, a simple explanation of plastic strain formation around the pool readily suggests itself. This explanation takes into account the substantial amount of shear strain measured during these experiments, whereas previous work has usually failed to recognize that this shearing even occurs.

The welding thermal strain pattern, as pointed out in the literature survey, depends on the temperature distribution around the moving weld pool. Compare the elongated 'teardrop' isotherms characteristic of welding heat flow with the concentric circle isotherms of a stationary heat source. The two cases are shown graphically in Fig. 9. In Fig. 9(a) the hot metal immediately surrounding the stationary heat source is restrained from expanding freely by the cooler metal further from the heat source. This restraint is uniform on all sides, and the resulting stress pattern caused by this restrained free expansion is thus uniform. As the heat input increases and the hottest material begins to yield in compression, the metal near the heat source will be compressed equally on all sides, and no net shifting of this region will occur.

However, the moving heat source situation in Fig. 9(b) is not so simple. Although the temperature profile through the arc in the X-direction is symmetrical around the weld centerline, the temperature profile in the Y-direction is distinctly asymmetrical. This is clearly shown by the recorder traces in Fig. 5 and by the temperature gradients measured from these traces in Table 2. Thermal stresses will be caused by this temperature distribution, just as in the stationary heat source example, but for the moving heat source, the compressive stresses will be much more intense in front of the arc than behind it, due to the much steeper temperature gradients there. This asymmetry of compressive stresses means that when plastic flow occurs, there will be a net shifting of metal rearward, so as to reduce the unbalanced front-to-rear stress pattern.

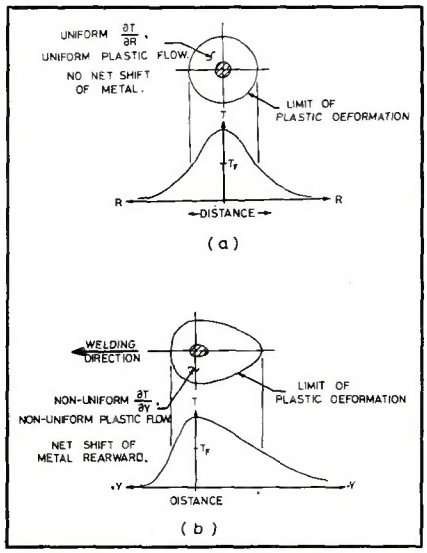

Fig. 9 — Comparison of thermal effects for a stationary and a moving heat source. The different temperature distributions give rise to different shapes and characteristics of the region where plastic flow takes place

The amount of shifting will clearly be dependent on the high temperature plastic behavior of the base metal as well as on the temperature distributions near the weld pool, but a detailed study of such behavior is beyond this paper. The non-quantitative simplification, that the alloy yields and flows more easily as temperature increases, is adequate for the present discussion.

These ideas can now be used to explain the variation in the strain patterns caused by changing welding conditions. The discussion is illustrated by Fig. 10, showing the relative sizes of plastic flow regions around a weld pool with different welding conditions. Figures 10(a) and 10(b) compare both high and low welding speeds while maintaining a constant weld bead size. Since the heating is concentrated closer to the pool, the thermal gradients are steeper for the high welding speed than for the low welding speed (see Fig. 6). The strains will also be higher immediately adjacent to the weld bead, but they will decrease rapidly away from the weld bead because of the rapid decrease in temperature and the corresponding increase in plastic flow resistance.

In the case of the low welding speed, however, lower thermal gradients occur which give rise to lower strain values near the weld and a more gentle decrease in strain away from the weld. The $\mathcal{E}_x$ and γ_{max} results show this travel speed effect. The effect of changing welding current at constant welding speed is shown in Fig. 10(b) and 10 (c). Although the thermal gradients are quite similar for the two cases, the temperature distribution in the high current weld will generally consist of higher temperatures at every point, thus leading to plastic straining over a larger area around the weld pool.

The strain graphs (Fig. 4) bring out several additional characteristics of welding plastic straining. The build-up of compressive normal strain in the X-direction indicates that powerful expansive forces around the arc are squeezing the nearby hot metal against the cooler restraining plate. The large shear strains caused by rearward displacement of the hot metal near the weld do not seem to be entirely the result of large compressive stresses in front of the arc. The fact that the cooling metal just behind the arc is still somewhat plastic while contracting means that it can therefore accommodate the expansion from ahead of the arc and contribute to this shearing. The combination of the $\mathcal{E}_x$ compression and the γ_{max} shearing causes a slight temporary bending of the originally straight lines which were parallel to the Y-axis. This bending only occurs to accommodate the build-up of compressive $\mathcal{E}_x$ strains, however, and it quickly disappears. The rearward bending of originally straight lines which were parallel to the X-axis is much greater, however, and is a permanent feature of the completed weld.

Not all of the compressive strain causes in-plane plastic flow. Prokhorov et al[14] and Chihoski[11] point out that the base metal near the weld thickens somewhat. Although the effect was not specifically measured during this work, some preliminary work showed this thickening quite clearly because it causes the plane of the surface to deflect slightly. Moiré gratings which were at first thought to have been destroyed by heat were later found to be in perfect condition except that bulging caused them to reflect normal illumination slightly off-center, giving a dark region of very poor fringe contrast in the movie films. Compressive upsetting is also evident in Fig. 7, where the hot metal under the fusion zone has been deformed.

Conclusions

1. The projected-grating grid-analyzer moiré fringe techniques described here are capable of accurately measuring the dynamic plastic strain patterns around a moving welding arc and solidifying weld bead.

2. Dynamic plastic strain patterns from a series of welds in an Al-Mg alloy show that large shear strains accompany the welding process. The planes of maximum shear strain are oriented almost exactly parallel and perpendicular to the direction of welding. This shearing displaces the metal near the weld rearward.

3. A theory of plastic strain formation during welding has been presented. The main feature of this theory is that the extent of the region of plastic flow near the weld and the amount of deformation in this region are directly related to the temperature distribution in the base metal.

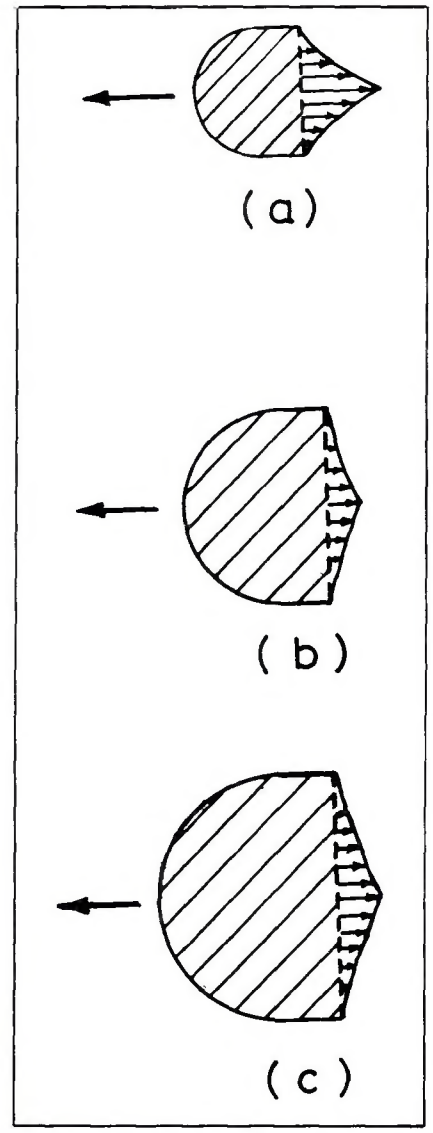

Fig. 10 — The relative amounts and distribution of plastic flow occurring around welds under three different conditions: (a) high welding speed; (b) low welding speed, low current; (c) low welding speed, high current. The arrows at the right of each diagram show the amount of rearward deformation taking place. The arrows at the left indicate the welding direction

Acknowledgments

Most of the financial support for this work was provided by the Ministry of Defense, Procurement Executive. Laboratory facilities were provided by the Metallurgy Department, University of

Strathclyde, Glasgow, Scotland (head of department Prof. P. Grieveson). The author is indebted to his thesis supervisor Mr. J. C. Borland for his encouragement and helpful discussions.

References

1. Okerblom, N. O. *The Calculations of Deformations of Welded Metal Structures,* translated from Russian (Mashgiz, 1955) by Her Majesty's Stationary Office, London, 1958.

2. Goodier, J. N., "Thermal stresses and deformation," *Journal of Applied Mechanics, 24,* no. 9, September, 1957. pp. 467-474.

3. Tall, L., "Residual stresses in welded plates — a theoretical study," *Welding Journal, 43,* no. 1, January, 1964. pp. 10s-23s.

4. Christensen, N., Davies, V. de L., Gjermundsen, K., "Distribution of temperatures in arc welding," *British Welding Journal, 12,* no. 2, February, 1965. pp. 54-75.

5. Myers, P. S., Uyehara, O. A., Borman, G. L., "Fundamentals of heat flow in welding," *Welding Research Council Bulletin 123,* July, 1967.

6. Kazimirov, A. A., Nedoseka, A. Ya., "The residual stresses and distortion which develop when the AMg5V alloy is welded," *Automatic Welding,* 1962, no. 10. pp. 13-17.

7. Boulton, N. S., Lance Martin, H. E., "Residual stresses in arc-welded plates," *Proceedings of the Institution of Mechanical Engineers, 133,* 1936. pp. 295-239.

8. Prokhorov, N. N., Nikol. Prokhorov, N., "Calculating welding deformations with electronic digital computers," *Automatic Welding,* 1966, no. 7. pp. 37-43.

9. Makhnenko, V. I., Shekera, V. M., "Effect of metal thickness on the nature of the stressed and strained state in it when subjected to a rapidly moving source of heat," *Welding Production, 18,* no. 7, July, 1971. pp. 1-5.

10. Masubuchi, K., Ich, N. T., "Computer analysis of degree of constraint of practical butt joints," *Welding Journal, 49,* no. 4, April, 1970. pp. 166s-176s.

11. Chihoski, R. A., "The character of stress fields around a weld arc moving on aluminum sheet," *Welding Journal, 51,* no. 1, January, 1972. pp. 9s-18s.

12. Dawes, M. G., "Residual stresses — Part 2: Stresses and strains — measurement," *The Welding Institute Research Bulletin, 9,* no. 4, April, 1968. pp. 98-103.

13. Makhneko, V. I., Velikoivanenko, E. A., Shekera, V. M., "Kinetics of the stressed and strained state in sheet metal when cracks are welded up," *Automatic Welding, 23,* no. 2, February, 1970. pp. 36-40.

14. Prokhorov, N. N., Osokina, T. N., Prokhorov (Jr.), N. N., "Plastic strain distribution in welded joints," *Welding Production, 17,* no. 8, August, 1970. pp. 17-20.

15. Dantu, P., "Extension of the moiré method to thermal problems," *Experimental Mechanics, 4,* no. 3, March, 1964. pp. 64-69.

16. Cargill, J., "Measuring strains under welds by the moiré fringe technique," *Journal of the British Society for Strain Measurement, 6,* no. 1, January, 1970. pp. 6-13.

17. Dyatlov, V. I., Sidoruk, V. S., "The effects of the welding technique on the formation of longitudinal hot cracks," *Automatic Welding,* March, 1966. pp. 21-26.

18. Dechaene, R., De Cock, J., De Caluwe, M., "Measurement of transient thermal plastic strains," *Journal of the British Society for Strain Measurement, 4,* no. 4, October, 1968. pp. 1-7.

19 Soete, W., et. al., "Exhaustion of ductility by hot straining or welding," International Institute of Welding Document X-431-67.

20. Kasatkin, B. S., Lobanov, L. M., "The thermal stresses caused in plates by spot sources of heat," *Automatic Welding,* 1965, no. 6. pp. 6-11.

21. Kasatkin, B. S., Lobanov, L. M., Tkachuk, G. I., "The stressed state in circular welds in a single plane investigated by the photoelasticity method," *Automatic Welding, 23,* no. 12, December, 1970. pp. 40-43.

22. Johnson, L. D., "A moiré fringe analysis of strains during welding and their relation of solidification cracking," Ph.D. thesis, Metallurgy Department, University of Strathclyde, Glasgow GI 1XN, Scotland, June, 1972.

23. Johnson, L. D., "Moiré techniques for measuring strains during welding," to be published in *Experimental Mechanics* at about the same time as this article appears.

24. Theocaris, P. S., *Moiré Fringes in Strain Analysis,* Permagon Press, London, 1969.

25. Parks, V. J., Durelli, A. J., "Various forms of the strain-displacement relations applied to experimental strain analysis," *Experimental Mechanics, 4,* no. 2, February, 1964. pp. 37-47.